Optics Letters

Improved performance of pure red perovskite light-emitting devices based on $CsPb(Br_{1-x}I_x)_3$ with variable content of iodine and bromine

Shuang Guo,[1] Yue-Feng Liu,[1,3] Yu-Shan Liu,[1] Jing Feng,[1] and Hong-Bo Sun[1,2,4]

[1]State Key Laboratory of Integrated Optoelectronics, College of Electronic Science and Engineering, Jilin University, Changchun 130012, China
[2]State Key Laboratory of Precision Measurement Technology and Instruments, Department of Precision Instrument, Tsinghua University, Haidian, Beijing 100084, China
[3]e-mail: yfliu23@jlu.edu.cn
[4]e-mail: hbsun@tsinghua.edu.cn

Received 23 March 2020; revised 12 April 2020; accepted 12 April 2020; posted 13 April 2020 (Doc. ID 393288); published 6 May 2020

All-inorganic cubic $\alpha-CsPbI_3$ perovskite for red perovskite light-emitting device (PeLED) applications is suffering from a phase transition. Unstable black α phase tends to transit to yellow δ phase under ambient conditions, which results in poor performance of the $CsPbI_3$-based PeLEDs. Partial replacement of iodine anion with a comparatively smaller bromine anion in the perovskite film can effectively adjust the Goldschmidt tolerance factor and stabilize the α-phase. A phase-stable $CsPb(Br_{1-x}I_x)_3$ perovskite has been obtained at low annealing temperature of 50°C by tuning the iodine-to-bromine ratios. A PeLED with pure red emission based on the $CsPb(Br_{0.43}I_{0.57})_3$ perovskite has been demonstrated. The maximum luminance and efficiency were 2200 cd/m^2 and 0.38 cd/A, respectively. Moreover, the PTAA layer was introduced between the PEDOT:PSS and perovskite film to improve the surface morphologies of perovskite. As a result, red PeLEDs with a maximum luminance of 2765 cd/m^2 have been achieved.

https://doi.org/10.1364/OL.393288

Metal halide perovskite has demonstrated great potential in light-emitting devices (LEDs) because of its high fluorescence quantum efficiency, adjustable luminescence spectrum, high color purity, excellent photoelectric characteristics, and facile solution processability [1–4]. Snaith and Friend *et al.* reported organic–inorganic hybrid lead halide perovskite LEDs (PeLEDs) in 2014 first [5]. But, external quantum efficiency (EQE) was low and just 0.1%. Various efforts have been conducted to improve the hybrid PeLEDs performance. They have shown rapidly increased EQE exceeding 20% [6–8]. Unfortunately, the poor inherent environmental and thermal stability of the hybrid PeLEDs has been an obstacle to their further developments and applications [9–14]. Compared with organic–inorganic hybrid perovskites, all-inorganic perovskites ($CsPbX_3$, X = Cl, Br, I) with higher stability show great potential in the field of optoelectronics [15,16]. Song *et al.* used the all-inorganic $CsPbX_3$ quantum dots for the first time to achieve blue, green, and yellow PeLEDs successfully. The maximum brightness and EQE of three color PeLEDs were 742 cd/m^2, 946 cd/m^2, and 528 cd/m^2 and 0.07%, 0.12%, and 0.09%, respectively [15]. Ling *et al.* incorporated polyethylene oxide (PEO) in $CsPbBr_3$, making the perovskite film grains smaller and smoother without pinholes, achieving green full inorganic PeLEDs with brightness and EQE reaching 53, 525 cd/m^2 and 4.26%, respectively [16].

Although over 10% EQE has been demonstrated for $CsPbBr_3$-based all-inorganic PeLEDs with green emission, it is still a challenge to achieve stable and efficient red PeLEDs, which hinder the application of the PeLEDs in both solid-state lighting and full-color displays [17,18]. The all-inorganic cubic $\alpha-CsPbI_3$ perovskite for red PeLED applications is suffering from a phase transition. Unstable black α phase tends to transit to yellow δ phase under ambient conditions, which results in poor performance of the $CsPbI_3$-based PeLEDs. Black cubic $\alpha-CsPbI_3$ perovskite is formed only under high temperature conditions [19]. Many efforts have been focused on fabricating and stabilizing the black perovskites at low temperature. Multiple quantum well (MQW) structures facilitate α phase formation. In 2017, Zhang *et al.* prepared a red PeLED with high efficiency based on a MQW structure. The maximum brightness and maximum EQE of 440 cd/m^2 and 3.7% have been achieved [20]. In 2018, they reported a maximum EQE of 12.7% by adjusting the width of the quantum wells [21]. Subsequently, Chiba *et al.* achieved a fairly efficient red PeLED with a peak EQE of 21.3% prepared with anion exchange from $CsPbBr_3$ using oleylammonium iodide in late 2018 [6], which is the maximum efficiency reported so far. Although the efficiency of the red PeLED has been improved significantly, the brightness has lagged far behind that of the green PeLED. In particular, the maximum brightness of the all-inorganic pure red PeLED having better stability is only 2671 cd/m^2 [22].

It has been reported that the PeLEDs based on nonstoichiometric perovskite films perform better [23]. Partial replacement of iodine anion with a comparatively akin bromine anion stabilizes black perovskites, which has been demonstrated as an

effective method to improve the stability of the red PeLEDs. Meanwhile, the light emission from the $CsPbI_3$ with the bandgap of 1.73 eV could be modified from deep red to pure red through introducing Br into $CsPbI_3$ perovskites and tuning the iodine-to-bromine ratios. In this work, α-phase $CsPb(Br_{1-x}I_x)_3$ perovskite at a low temperature of 50°C has been obtained by using nonstoichiometric precursor solutions with the excess CsBr remaining within the perovskite film. A PeLED with pure red emission based on the $CsPb(Br_{0.43}I_{0.57})_3$ perovskite has been demonstrated. The maximum luminance and efficiency were 2200 cd/m^2 and 0.38 cd/A, respectively. Moreover, the poly [bis(4-phenyl)(2,4,6-trimethylphenyl) amine] (PTAA) layer was introduced between the poly(3, 4-ethylenedioxythiophene) polystyreneulfonate (PEDOT:PSS) and perovskite films to improve the crystal quality. As a result, red PeLEDs with a maximum luminance of 2765 cd/m^2 have been achieved.

CsBr (99.999%) and PbI_2 (99.999%) were picked out from Sigma Aldrich. PEDOT:PSS and TPBi [1, 3, 5-tris (2-N-phenylbenzimidazolyl)-benzene] were purchased from Xi'an Polymer Light Technology Corp. All materials have been employed as received without further purification. The precursor solutions of perovskite films with different halide atomic ratios were achieved through dissolving CsBr and PbI_2 with different molar ratios in a mixed solvent of N, N-dimethylformamide (DMF) and dimethyl sulfoxide (DMSO) with 15 wt. % concentration, where the volume ratio of DMF to DMSO was 5:1. The four perovskite precursor solutions of $CsPb(Br_{0.46}I_{0.54})_3$, $CsPb(Br_{0.45}I_{0.55})_3$, $CsPb(Br_{0.43}I_{0.57})_3$, and $CsPb(Br_{0.33}I_{0.67})_3$ films were from CsBr and PbI_2 with the molar ratios of 1.3:1, 1.5:1, 1.7:1, and 1.9:1, respectively. The four precursor solutions were stirred at 50°C overnight. Then, after these solutions were allowed to stand for an hour, precipitates appeared in these CsBr-rich solutions, and the supernatants were separated and filtered for preparing perovskite films.

Patterned ITO glass was selected as the substrate. The substrate was precleaned by ultrasonic baths in acetone, ethanol, and deionized water sequentially and dried in an oven at 95°C. Then, the substrate was conducted in oxygen plasma for 5 min. The PTAA solution (6 mg/ml) was deposited by spin-coating (6000 rpm for 30 s) on substrate, followed by an annealing process at 90°C for 10 min. After that, the PEDOT:PSS layer was fabricated in condition of spin-coating at 6000 rpm for 30 s and annealing at 120°C for 10 min. Next, the substrate was loaded into a glovebox to fabricate the perovskite film. The precursor solutions were spin-coated at 5000 rpm for 30 s and annealed at 50°C for 30 min. Finally, all substrates were moved into a chamber with high vacuum of 5×10^{-4} Pa to deposit TPBi (50 nm), LiF (0.6 nm), and Al (100 nm) by evaporation.

Surface morphology of perovskite films was characterized using scanning electron microscopy (SEM, JEOL JSM-7500 F). X-ray diffraction (XRD) measurements were obtained from a Rigaku D/MAX 2550 diffractometer with Cu Kα radiation ($\lambda = 1.5418$ Å) to study the crystal structure of perovskite films. The current density-voltage-luminance (J-V-L) properties and electroluminescence (EL) spectra of the PeLEDs were measured using a Keithley 2400 source measurement and a Photo Research PR655 spectrophotometer. X-ray photoelectron spectroscopy (XPS, ESCALAB 250) was used to analyze the element species and atomic ratio of the perovskite films prepared.

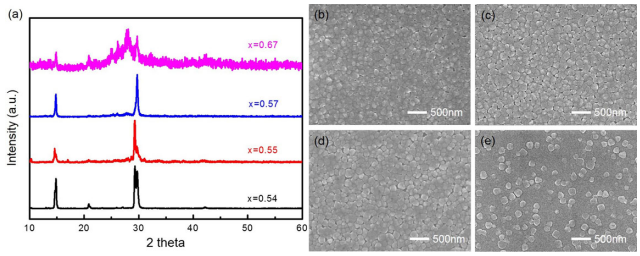

Fig. 1. Characterizations of the $CsPb(Br_{1-x}I_x)_3$ films with different stoichiometry. (a) XRD spectra of $CsPb(Br_{1-x}I_x)_3$ films. SEM images of (b) $CsPb(Br_{0.46}I_{0.54})_3$ film, (c) $CsPb(Br_{0.45}I_{0.55})_3$ film, (d) $CsPb(Br_{0.43}I_{0.57})_3$, and (e) $CsPb(Br_{0.33}I_{0.67})_3$.

The $CsPb(Br_{1-x}I_x)_3$ perovskite films with varying iodide concentration "x" were prepared by spin-coating nonstoichiometric perovskite precursor solution on substrates. First, XRD spectroscopy was measured to characterize the crystal structure and confirm the formation of α-phase perovskite for the perovskite films with various iodide concentration, as shown in Fig. 1(a). Known by the Goldschmidt tolerance factor, the iodide ion is too large to form a stable cubic perovskite phase with cesium ions and lead ions. The mixing of halogen atoms is an effective way to change the Goldschmidt tolerance factor and improve the phase stability of the perovskite. It can be seen from the XRD pattern that the perovskite crystals cannot be formed with a large iodide concentration ($x = 0.67$). With the decreasing of the iodide concentration ($x = 0.57$, 0.55, 0.54), the XRD pattern of the perovskite films shows significant peaks at 15° and 30°. These peaks correspond to the (100) and (200) crystal faces of α-phase perovskite, which indicate the formation of α-phase perovskite. The XRD pattern of the $CsPb(Br_{1-x}I_x)_3$ perovskite films with $x = 0.54$ and 0.55 shows a peak splitting at the diffraction peak of 30°, indicating a lower symmetry and a distorted cubic structure [24]. Meanwhile, a small amount of inconspicuous peaks appear between 15° and 30°, which indicate the presence of noncubic perovskite phases. An optimal cubic perovskite crystal structure is formed when $x = 0.57$. It can be concluded from the above results that stable α-phase perovskite has been formed at low temperatures (50°C) by introducing bromine atoms and adjusting the proportion of halogen atoms. In order to analyze the surface morphology of the perovskite films, SEM measurements were performed. Figures 1(b)–1(e) show the SEM images of $CsPb(Br_{1-x}I_x)_3$ perovskite films with different x values. The $CsPb(Br_{0.43}I_{0.57})_3$ film exhibits better morphologies compared to the other three films, higher film coverage, and homogeneous grain size with fewer grain boundaries.

Metallic Pb atoms produced in perovskite films can greatly enhance nonradiative recombination rate and reduce radiation recombination rate [25], reducing the luminescence properties of PeLEDs. However, Pb atoms are easily generated in lead halide perovskite films owing to the undesigned losses of halogen atoms and incomplete precursor reaction. Element species and atomic ratios of perovskite films were analyzed by XPS. The survey spectra show main peaks of Cs 3d, Pb 4f, Br 3d, and I 3d [Fig. 2(a)]. By adjusting the stoichiometry of perovskite precursors, we successfully inhibited the formation of lead atoms on perovskite films, as evidenced by XPS Pb 4f spectra [Fig. 2(b)].

In order to investigate the effect of halogen atomic ratios on the performance of PeLED, red PeLEDs with different halogen

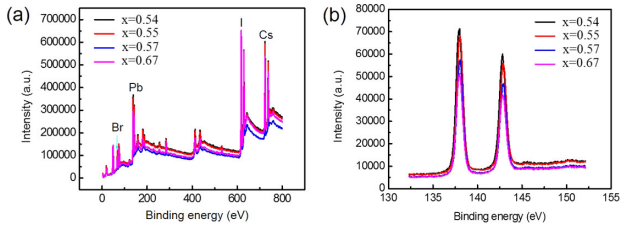

Fig. 2. XPS spectra of $CsPb(Br_{1-x}I_x)_3$ films. (a) Survey spectra. (b) High resolution XPS spectra of Pb 4f.

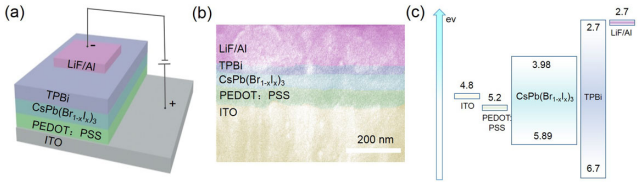

Fig. 3. Schematic illustrations of the PeLEDs. (a) Device structure, (b) cross-sectional SEM images, and (c) energy band diagram of the PeLEDs.

atomic ratios have been fabricated. The structure of the PeLEDs is ITO (200 nm)/PEDOT:PSS (50 nm)/$CsPb(Br_{1-x}I_x)_3$ (50 nm)/TPBi (50 nm)/LiF (0.5 nm)/Al (120 nm). The stacked structure and cross-section SEM images of the PeLEDs are shown in Figs. 3(a) and 3(b). Figure 3(c) shows the energy-level diagram of the $CsPb(Br_{0.43}I_{0.57})_3$ PeLED, in which the energy level of the $CsPb(Br_{0.43}I_{0.57})_3$ film was obtained by combining the ultraviolet photoelectron spectroscopy (UPS) and absorption spectrum. The EL performances of the red PeLEDs based on the perovskite films with different halogen atomic ratios are shown in Fig. 4. As expected, the PeLEDs based on the $CsPb(Br_{0.43}I_{0.57})_3$ perovskite films exhibit highest luminance and efficiency because of their higher crystallinity and better surface morphology. Also, the turn-on voltage of the PeLED based on the $CsPb(Br_{0.43}I_{0.57})_3$ perovskite film is lower and just 2.5 V. Its maximum luminance, current efficiency, and EQE

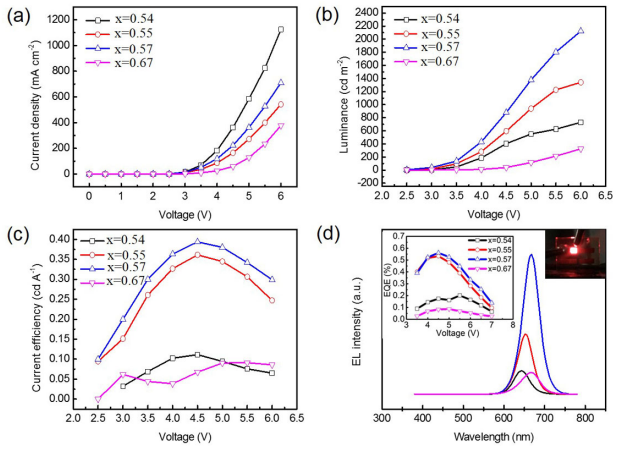

Fig. 4. EL performances of the PeLEDs based on the $CsPb(Br_{1-x}I_x)_3$ with various iodide concentration "x." (a) Current density, (b) luminance, (c) current efficiency versus voltage, and (d) EL spectra. The insets in (d) show EQE–V curves and a photograph of the $CsPb(Br_{0.43}I_{0.57})_3$-based PeLED working at 5 V.

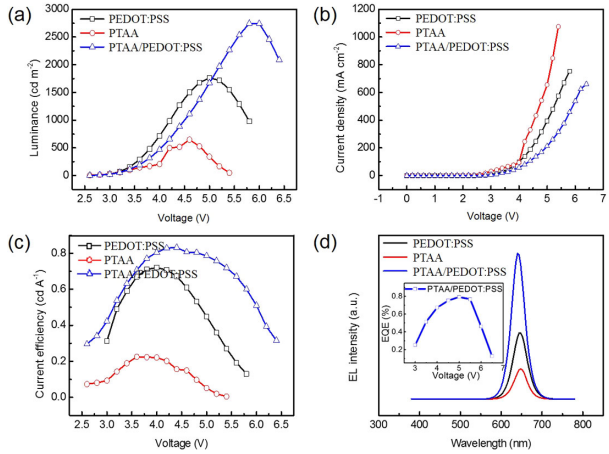

Fig. 5. EL performances of the PeLEDs based on different hole transport layers. (a) Luminance, (b) current density, (c) current efficiency versus voltage characteristic, and (d) EL spectra. The inset in (d) shows EQE–V curve of the PeLED based on PTAA/PEDOT:PSS HTL.

can reach 2200 cd/m^2 [Fig. 4(b)], 0.38 cd/A [Fig. 4(c)], and 0.56% [the inset in Fig. 4(d)] respectively. The EL spectra of the PeLEDs show a blueshift with the decreasing of the iodide concentration Fig. 3(d). The peak wavelength is decreased from 672 nm for $x = 0.67$ to 644 nm for $x = 0.54$. Pure red emission with central wavelength at 664 nm can be obtained for the PeLEDs with the optimized iodide concentration of $x = 0.57$. The pure and uniform red light emission from the PeLED based on the $CsPb(Br_{0.43}I_{0.57})_3$ perovskite film can be observed from the photograph of the operating device [inset in Fig. 4(d)].

To further improve device performance, a thin PTAA layer was introduced between ITO and PEDOT:PSS to form a double-layer hole transport structure. PTAA is an excellent hole transporting material and commonly used to improve the performance of perovskite solar cells. The PeLEDs based on the double-layer hole transport layer exhibit enhanced EL performance compared to the devices with single layer of PEDOT:PSS or PTAA (Fig. 5). The maximum luminance and current efficiency are 2765 cd/m^2 and 0.84 cd/A, respectively. A maximum EQE of 0.8% has been achieved [the inset in Fig. 5(d)].

The surface morphology of the perovskite films spin-coated on the different hole transport layers was characterized by SEM to verify the enhancement of the EL performance (Fig. 6). As can be seen from Figs. 6(a) and 6(b), the double-layer structure can effectively improve the surface topography of the perovskite film compared to the conventional hole transport layer PEDOT:PSS. The perovskite spin-coated on the double-hole transport layer (PTAA/PEDOT:PSS) leads to smaller crystal size, reduced pinholes, and increased fraction of surface

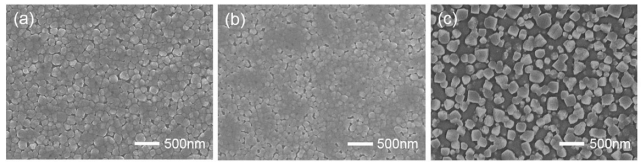

Fig. 6. SEM images of the $CsPb(Br_{0.43}I_{0.57})_3$ films spin-coated on different hole transport layers of (a) PEDOT:PSS, (b) PTAA/PEDOT:PSS, and (c) PTAA.

coverage. This is due to the better film-forming properties of PEDOT:PSS spin-coated on PTAA, which improves the quality of surface morphology. The surface morphology of the perovskite film directly spin-coated on the PTAA layer also was characterized. It can be seen from Fig. 6(c) that the crystal grains and the pores are larger, resulting in a larger current density of the device based on the PTAA hole transport layer.

In conclusion, phase-stable $CsPb(Br_{1-x}I_x)_3$ perovskite at a low annealing temperature of 50°C has been achieved by partial replacement of iodine anion with a relatively smaller Br anion and tuning the iodine-to-bromine ratios. The PeLEDs based on the $CsPb(Br_{0.43}I_{0.57})_3$ perovskite films exhibit higher luminance and current efficiency because of their higher crystallinity and better surface morphology. The maximum luminance of 2200 cd/m^2, current efficiency of 0.38 cd/A, and pure red emission with central wavelength at 664 nm were obtained. Moreover, the crystal morphologies were further improved by introducing a PTAA layer between the PEDOT:PSS and perovskite layers. As a result, red PeLEDs with a maximum luminance of 2765 cd/m^2 have been achieved.

Funding. National Key Research and Development Program of China; National Natural Science Foundation of China (2017YFB0404500, 61825402, 61675085, 61805096).

Disclosures. The authors declare no conflicts of interest.

REFERENCES

1. W. Hu, H. Cong, W. Huang, Y. Huang, L. Chen, A. Pan, and C. Xue, Light Sci. Appl. **8**, 106 (2019).
2. C. H. Kang, I. Dursun, G. Liu, L. Sinatra, X. Sun, M. Kong, J. Pan, P. Maity, E. N. Ooi, T. K. Ng, O. F. Mohammed, O. M. Bakr, and B. S. Ooi, Light Sci. Appl. **8**, 94 (2019).
3. S. B. Kang, J.-H. Kim, M. H. Jeong, A. Sanger, C. U. Kim, C.-M. Kim, and K. J. Choi, Light Sci. Appl. **8**, 121 (2019).
4. D. Chen and X. Chen, J. Mater. Chem. C **7**, 1413 (2019).
5. Z. K. Tan, R. S. Moghaddam, M. L. Lai, P. Docampo, R. Higler, F. Deschler, M. Price, A. Sadhanala, L. M. Pazos, D. Credgington, F. Hanusch, T. Bein, H. J. Snaith, and R. H. Friend, Nat. Nanotechnol **9**, 687 (2014).
6. T. Chiba, Y. Hayashi, H. Ebe, K. Hoshi, J. Sato, S. Sato, Y.-J. Pu, S. Ohisa, and J. Kido, Nat. Photonics **12**, 681 (2018).
7. K. Lin, J. Xing, L. N. Quan, F. P. G. de Arquer, X. Gong, J. Lu, L. Xie, W. Zhao, D. Zhang, C. Yan, W. Li, X. Liu, Y. Lu, J. Kirman, E. H. Sargent, Q. Xiong, and Z. Wei, Nature **562**, 245 (2018).
8. Y. Cao, N. Wang, H. Tian, J. Guo, Y. Wei, H. Chen, Y. Miao, W. Zou, K. Pan, Y. He, H. Cao, Y. Ke, M. Xu, Y. Wang, M. Yang, K. Du, Z. Fu, D. Kong, D. Dai, Y. Jin, G. Li, H. Li, Q. Peng, J. Wang, and W. Huang, Nature **562**, 249 (2018).
9. C. Wu, Y. Zou, T. Wu, M. Ban, V. Pecunia, Y. Han, Q. Liu, T. Song, S. Duhm, and B. Sun, Adv. Funct. Mater. **27**, 1700338 (2017).
10. P. Docampo and T. Bein, Acc. Chem. Res. **49**, 339 (2016).
11. A. Dualeh, P. Gao, S. I. Seok, M. K. Nazeeruddin, and M. Grätzel, Chem. Mater. **26**, 6160 (2014).
12. Y. Zhao and K. Zhu, Chem. Soc. Rev. **45**, 655 (2016).
13. T. Baikie, Y. Fang, J. M. Kadro, M. Schreyer, F. Wei, S. G. Mhaisalkar, M. Graetzel, and T. J. White, J. Mater. Chem. A **1**, 5628 (2013).
14. J. Feng, Y. F. Liu, Y. G. Bi, and H. B. Sun, Laser Photon. Rev. **11**, 1600145 (2017).
15. J. Song, J. Li, X. Li, L. Xu, Y. Dong, and H. Zeng, Adv. Mater. **27**, 7162 (2015).
16. Y. Ling, Y. Tian, X. Wang, J. C. Wang, J. M. Knox, F. Perez-Orive, Y. Du, L. Tan, K. Hanson, B. Ma, and H. Gao, Adv. Mater. **28**, 8983 (2016).
17. D. Yin, N. R. Jiang, Y. F. Liu, X. L. Zhang, A. W. Li, J. Feng, and H. B. Sun, Light Sci. Appl. **7**, 35 (2018).
18. R. Ding, F. X. Dong, M. H. An, X. P. Wang, M. R. Wang, X. B. Li, J. Feng, and H. B. Sun, Adv. Funct. Mater. **29**, 1807606 (2019).
19. B. Jeong, H. Han, Y. J. Choi, S. H. Cho, E. H. Kim, S. W. Lee, J. S. Kim, C. Park, D. Kim, and C. Park, Adv. Funct. Mater. **28**, 1706401 (2018).
20. S. Zhang, C. Yi, N. Wang, Y. Sun, W. Zou, Y. Wei, Y. Cao, Y. Miao, R. Li, Y. Yin, N. Zhao, J. Wang, and W. Huang, Adv. Mater. **29**, 1606600 (2017).
21. W. Zou, R. Li, S. Zhang, Y. Liu, N. Wang, Y. Cao, Y. Miao, M. Xu, Q. Guo, D. Di, L. Zhang, C. Yi, F. Gao, R. H. Friend, J. Wang, and W. Huang, Nat. Commun. **9**, 608 (2018).
22. J. N. Yang, Y. Song, J. S. Yao, K. H. Wang, J. J. Wang, B. S. Zhu, M. M. Yao, S. U. Rahman, Y. F. Lan, F. J. Fan, and H. B. Yao, J. Am. Chem. Soc. **142**, 2956 (2020).
23. Z. Wang, T. Cheng, F. Wang, S. Dai, and Z. Tan, Small **12**, 4412 (2016).
24. S. Dastidar, D. A. Egger, L. Z. Tan, S. B. Cromer, A. D. Dillon, S. Liu, L. Kronik, A. M. Rappe, and A. T. Fafarman, Nano Lett. **16**, 3563 (2016).
25. H. Cho, S.-H. Jeong, M.-H. Park, Y.-H. Kim, C. Wolf, C.-L. Lee, J. H. Heo, A. Sadhanala, N. Myoung, and S. Yoo, Science **350**, 1222 (2015).